70th International Astronautical Congress (IAC), Washington D.C., United States, 21-25 October 2019.

IAC-19-A6.2.3

A semi-analytical approach to low-thrust collision avoidance manoeuvre design

Juan Luis Gonzalo[a]*, Camilla Colombo[b], Pierluigi Di Lizia[c]

[a] *Postdoctoral research fellow, Department of Aerospace Science and Technology, Politecnico di Milano, Via la Masa 34, Milan, Italy 20156*, juanluis.gonzalo@polimi.it
[b] *Associate professor, Department of Aerospace Science and Technology, Politecnico di Milano, Via la Masa 34, Milan, Italy 20156*, camilla.colombo@polimi.it
[c] *Assistant professor, Department of Aerospace Science and Technology, Politecnico di Milano, Via la Masa 34, Milan, Italy 20156*, pierluigi.dilizia@polimi.it
* Corresponding Author

Abstract

The recent reductions in the cost of access to space and the introduction of smaller, more cost-effective platforms have spurred novel mission concepts ranging from small CubeSat-based experiments to large constellations. Inevitably, this will also lead to a notable increase in collision avoidance activities. Furthermore, an increasing number of satellites operate with low-thrust propulsion systems, which lack the last-time Collision Avoidance Manoeuvre (CAM) capabilities of traditional propulsion systems. Therefore, there is a clear need for the development of models and tools for the analysis and design of CAMs in the low-thrust context. Moreover, the large (and increasing) amount of Close Approaches (CA) to be analysed per day stresses the importance for these tools not only to be accurate but fast. This work presents a semi-analytical approach for the analysis and design of CAMs using low thrust. The model is based on the proximal motion equations and takes into consideration the effects of drag and solar radiation pressure and the low-thrust control acceleration. Averaged dynamics on Keplerian elements are used to obtain compact and efficient expressions, suitable for large simulation campaigns or on-board applications. Different figures of merit for the CAM are considered, mainly maximising miss distance. Another key aspect is the utilisation of the b-plane of the nominal encounter to analyse the dynamics of the deflected trajectory, exploiting its separation of phasing and geometry-change effects. Several test cases are presented, highlight the accuracy and computational efficiency of the approach and supporting the operational interest of this type of CAMs.

Keywords: Collision avoidance manoeuvre, Space Situational Awareness, low-thrust, semi-analytical methods, b-plane

Nomenclature

$\boldsymbol{a}$	Acceleration vector $[\mathrm{m/s^2}]$
a	Semimajor axis [km]
a_t	Tangential acceleration $[\mathrm{m/s^2}]$
b	Semiminor axis [km]
c_D	Drag coefficient $[-]$
c_R	Reflectivity coefficient $[-]$
e	Eccentricity $[-]$
E	Eccentric anomaly [deg]
E	Incomplete elliptic integral of the second kind
f	True anomaly [deg]
F	Incomplete elliptic integral of the first kind
h	Angular momentum $[\mathrm{m^2/s^2}]$
i	Inclination [deg]
k	Duration in revolutions of the low-thrust CAM
M	Mean anomaly [deg]
n	Mean motion $[\mathrm{s^{-1}}]$
p	Semilatus rectum [km]
$\boldsymbol{r}$	Position vector [km]
r	Radial distance [km]
t	Time [s]
T	Period for the nominal spacecraft orbit [s]
$\mathbf{u}_x$	Unit vector along direction x $[-]$
$\mathbf{v}$	Velocity vector $[\mathrm{m/s}]$
v	Velocity $[\mathrm{m/s}]$
$\boldsymbol{\alpha}$	Vector of Keplerian elements $[a, e, i, \Omega, \omega, M]$
α	Generic Keplerian element
δb	Deflection in the b-plane [km]
δx	Change in magnitude x due to the CAM
Δt_{CAM}	Duration of the low-thrust CAM [s]
Δt	Lead time of the CAM [s]
η	Axis perpendicular to the b-plane [km]
ζ	Time axis in the b-plane [km]
θ	Argument of latitude [deg]
μ	Earth's gravitational parameter $[\mathrm{km^3/s^2}]$
ξ	Geometry axis in the b-plane [km]
ω	Argument of perigee [deg]
Ω	Argument of the ascending node [deg]

Subscripts

CA	Close approach
f	Final point of the low-thrust manoeuvre
h	Out-of-plane component
i	Initial point of the low-thrust manoeuvre

n	Normal component
nom	Nominal value
num	Numerical solution
r	Radial component
sa	Semi-analytical solution
t	Tangential component
θ	Transversal component

Acronyms/Abbreviations

CA	Close approach
CAM	Collision avoidance manoeuvre
D	Debris
LEO	Low Earth Orbit
OD	Orbit determination
SC	Spacecraft
SRP	Solar radiation pressure
STM	State transition matrix

1. Introduction

Current and future trends for the scientific and commercial utilisation of near-Earth space depict an increasingly congested and complex scenario. Advances in different fronts such as the steady reductions in the cost of access to space thanks to new launch providers and the popularisation of rideshare missions, the introduction of more cost-effective platforms, and the increased interest in space activities by developing countries and private companies, have spurred novel mission concepts ranging from small CubeSat-based experiments to large constellations. Inevitably, this will come with a notable increase in collision avoidance activities. Furthermore, a sustainable development model will also require the adherence to end-of-life disposal policies, like the Inter-Agency Space Debris Coordination Committee guideline of 25 years maximum deorbit time for objects in low Earth orbit. This objective can be achieved in an efficient manner using passive deorbiting devices such as sails of tethers, but their large cross-sectional area further increases collision probability with nearby objects. Fortunately, effective CAMs by sails can be implemented for a sufficient warning time, compatible with current practices, assuming that the spacecraft has a certain level of attitude control during the deorbiting phase [1]. On the other hand, an increasing number of satellites are being equipped with ionic of Hall effect thrusters, due to their advantages in propellant consumption. Both sails and electric thrusters operate as low-thrust propulsion systems, delivering a small but continuous acceleration, as opposite to the classical impulsive propulsion systems. However, the reduced propellant consumption of these systems comes at the cost of lower control authority, hindering the implementation of last-minute CAMs and requiring a higher analysis effort from satellite operators.

Moving forward, there is a clear need to develop models and tools for the analysis and design of CAMs in the low-thrust context. Also, the large (and increasing) amount of CAs to be analysed per day stresses the importance for these tools not only to be accurate but fast. Aiming to address these needs, this work presents a semi-analytical solution for the analysis and design of CAMs using low thrust. This new model is part of the Manoeuvre Intelligence for Space Safety (MISS) software tool, currently being developed by the European Research Council-funded COMPASS project [2]. COMPASS pursues the goal of exploiting dynamical perturbations in order to tackle key problems in orbital mechanics. The CAM model is based on proximal motion equations and considers different forces, such as the effect of drag and solar radiation pressure and the low-thrust control acceleration. Averaged dynamics are used to obtain compact and efficient expressions, suitable for large simulation campaigns or on-board applications. Different figures of merits for CAMs are considered, mainly maximising miss distance or minimising collision probability. Another key aspect is the utilisation of the b-plane of the nominal encounter to analyse the dynamics of the deflected trajectory, exploiting its separation of phasing and geometry-change effects.

The paper is organised as follows. First, the CA scenario and CAM design problem under consideration are introduced in Section 2. Then, in Section 3 the dynamical model is presented, paying especial attention to the averaging process followed to obtain the semi-analytical expressions for modelling the changes in orbital elements due to the low-thrust CAM. A short paragraph is also devoted to the control strategies considered. Section 4 presents several numerical test cases, highlighting the accuracy and computational efficiency of the proposed approach and supporting the operational interest of this type of CAMs. Particularly, the effect of drag and SRP on the uncertainty evolution for bodies with large area-to-mass ratio is evaluated, a parametric analysis of a low-thrust CAM is provided, and some comments regarding CAMs by sails are presented. Finally, Section 5 draws conclusions and details the future works.

2. Problem statement

Let us consider two Earth-orbiting objects having a close approach at a time t_{CA}. One of them is a spacecraft equipped with a continuous, low-thrust propulsion system, while the other is a non-cooperative debris. The objective is to design a low-thrust CAM leading to either the maximisation of the miss distance or the minimisation of risk at t_{CA}. Note that the debris designation given here is generic and can refer to any Earth orbiting object, if it does not cooperate in the CAM (this can include another operative satellite).

To characterise the CA, the b-plane for the nominal encounter is used [3]. The b-plane has been successfully employed in previous works dealing with the design of CAMs and asteroid deflection missions [1][4], mostly

thanks to its property of separating the displacements related to phasing changes and orbit geometry changes into the so-called time axis ζ and geometry axis ξ, respectively. For a given nominal CA, the reference frame associated to the b-plane is centred at the position of the debris and has unity vectors $\{\mathbf{u}_\eta, \mathbf{u}_\xi, \mathbf{u}_\zeta\}$:

$$\mathbf{u}_\eta = \frac{\mathbf{v}_{SC} - \mathbf{v}_D}{\|\mathbf{v}_{SC} - \mathbf{v}_D\|}, \qquad \mathbf{u}_\xi = \frac{\mathbf{v}_D \times \mathbf{u}_\eta}{\|\mathbf{v}_D \times \mathbf{u}_\eta\|},$$
$$\mathbf{u}_\zeta = \mathbf{u}_\xi \times \mathbf{u}_\eta$$

where $\mathbf{v}_{SC}$ and $\mathbf{v}_D$ are the velocity vectors of spacecraft and debris, respectively.

Previous results obtained following a similar approach to the one proposed in this work but for impulsive CAMs, see [1], show that the orientation of optimal CAMs, either for maximum miss distance or minimum collision probability, tend to align with the tangential direction as the lead time between the manoeuvre and the CA increases (particularly, for lead times greater than a period of the spacecraft). The b-plane analysis of the CAM reveals that this behaviour is associated with a displacement dominant along the time axis, leveraging the change in phasing. However, while this behaviour is very clear for the maximum deviation CAM, a more irregular evolution is observed for the minimum collision probability one, the reason being that uncertainties also tend to grow along the time axis. Considering these results, and that tangential thrusting provides optimal instantaneous energy change under continuous low thrust, in the following a tangential thrust control strategy is assumed.

3. Dynamical model

Assuming that the change in the spacecraft orbit due to the CAM is small, one can express the deviation with respect to the nominal orbit using the linearized relative motion equations [5]:

$$\delta r_r \approx \frac{r}{a}\delta a + \frac{a\, e \sin f}{\sqrt{1-e^2}}\delta M - a\cos f\, \delta e \tag{1}$$

$$\delta r_\theta \approx \frac{r}{(1-e^2)^{3/2}}(1+e\cos f)^2 \delta M + r\delta\omega + \frac{r\sin f}{1-e^2}(2+e\cos f)\delta e + r\cos i\ \delta\Omega \tag{2}$$

$$\delta r_h \approx r(\sin\theta\, \delta i - \cos\theta \sin i\, \delta\Omega) \tag{3}$$

or in matrix form:

$$\delta\mathbf{r} \approx \mathbf{A}_r \delta\boldsymbol{\alpha}$$

where $\boldsymbol{\alpha} = [a, e, i, \Omega, \omega, M]$ is the vector of Keplerian elements and $\delta\boldsymbol{\alpha}$ its changes at t_{CA} due to the CAM. The evolution of $\boldsymbol{\alpha}$ can be obtained through Gauss' planetary equations, which have to be integrated numerically for a general perturbing acceleration $\boldsymbol{a}(t)$.

In the following, a set of semi-analytical formulas for the variation of the orbital elements due to a constant tangential thrust are presented. Let us first consider the Gauss' planetary equations for a constant tangential perturbing acceleration [6]:

$$\begin{aligned}
\frac{\mathrm{d}a}{\mathrm{d}t} &= \frac{2a^2 v}{\mu} a_t \\
\frac{\mathrm{d}e}{\mathrm{d}t} &= \frac{2(e+\cos f)}{v} a_t \\
\frac{\mathrm{d}i}{\mathrm{d}t} &= 0 \\
\frac{\mathrm{d}\Omega}{\mathrm{d}t} &= 0 \\
\frac{\mathrm{d}\omega}{\mathrm{d}t} &= \frac{2\sin f}{ev} a_t \\
\frac{\mathrm{d}M}{\mathrm{d}t} &= n - \frac{2b}{eav}\left(1 + \frac{e^2 r}{p}\right)\sin f\, a_t
\end{aligned} \tag{4}$$

where a_t is the magnitude of the low-thrust acceleration. The sign of a_t can be either positive of negative depending on whether the acceleration is oriented along the velocity vector or opposite to it, respectively. Expressing Eqs. (4) in terms of the eccentric anomaly E they take the form [7][8]:

$$\begin{aligned}
\frac{\mathrm{d}a}{\mathrm{d}E} &= a_t \frac{2a^3}{\mu}\sqrt{1-e^2\cos^2 E} \\
\frac{\mathrm{d}i}{\mathrm{d}E} &= 0 \\
\frac{\mathrm{d}\Omega}{\mathrm{d}E} &= 0 \\
\frac{\mathrm{d}\omega}{\mathrm{d}E} &= a_t \frac{2a^2\sqrt{1-e^2}}{\mu e}\sqrt{\frac{1-e\cos E}{1+e\cos E}}\sin E \\
\frac{\mathrm{d}M}{\mathrm{d}E} &= (1-e\cos E)\left(1 - a_t \frac{2a^2(1-e^3\cos E)\sin E}{e\mu\sqrt{1-e^2\cos^2 E}}\right)
\end{aligned} \tag{5}$$

where the relation between E and t has been approximated as:

$$\frac{\mathrm{d}E}{\mathrm{d}t} \approx \sqrt{\frac{\mu}{a^3}}\frac{1}{1-e\cos E} \tag{6}$$

obtained by taking the derivative with respect to E in Kepler's equation. Assuming that all elements except E are constant over one revolution and integrating in E the right-hand side of Eqs. (5), the following primitives are reached:

$$\begin{aligned}
H_a(E) &= a_t \frac{2a^3\sqrt{1-e^2}}{\mu}\,\mathrm{E}\left[E, -\frac{e^2}{1-e^2}\right] \\
H_e(E) &= a_t \frac{2a^2(1-e^2)}{\mu e}\left[\frac{1}{2}\ln\left(\frac{\sqrt{1-e^2\cos^2 E} + e\sin E}{\sqrt{1-e^2\cos^2 E} - e\sin E}\right)\right. \\
&\quad - \frac{1}{\sqrt{1-e^2}}\mathrm{F}\left[E, -\frac{e^2}{1-e^2}\right] \\
&\quad \left. + \sqrt{1-e^2}\,\mathrm{E}\left[E, -\frac{e^2}{1-e^2}\right]\right] \\
H_i(E) &= H_\Omega(E) = 0 \\
H_\omega(E) &= a_t \frac{2a^2\sqrt{1-e^2}}{\mu e}\left[2\,\mathrm{asin}\sqrt{\frac{1-e\cos E}{2}}\right. \\
&\quad \left. - \sqrt{1-e^2\cos^2 E}\right]
\end{aligned} \tag{7}$$

where F[·,·] and E[·,·] are the incomplete elliptic integrals of the first and second kind, respectively [6]. The mean variation of each Keplerian element over one revolution then takes the form:

$$\Delta\alpha = H_{\alpha}(2\pi) - H_{\alpha}(0) \tag{8}$$

Note that evaluating Eq. (8) for ω leads to $\Delta\omega = 0$, so only semimajor axis and eccentricity experience secular changes under a continuous tangential thrust. These expressions assume that a_t remains constant over one revolution, which is a good first approximation for low-thrust propulsion systems. The value of a_t at each revolution could be updated by accounting for the mass loss using the expressions provided by Huang et al. in [9], but given the short time span typical of CAMs the effect of mass variations is neglected in the current work. On the other hand, eclipses can also affect a_t due to restrictions on the power available for the propulsion system. Equation (8) can be adapted to the case where the low-thrust propulsion system is off during eclipses by evaluating it between the eccentric anomalies corresponding to the exit from and entry into the eclipse region (that is, over the arc where the thruster is active), instead of between 0 and 2π. In that case, $\Delta\omega$ will no longer be zero in general.

Equations (7) and (8) approximate the variations of all orbital elements in $\boldsymbol{\alpha}$, except for M, over one revolution, that is, $\delta a = \Delta a$, $\delta e = \Delta e$, $\delta i = \Delta i = 0$, $\delta\Omega = \Delta\Omega = 0$, and $\delta\omega = \Delta\omega = 0$. For a low-thrust CAM lasting k revolutions, the total change in $\boldsymbol{\alpha}$ can be computed by evaluating $\Delta\boldsymbol{\alpha}$ sequentially for each revolution, updating the values of the orbital elements at the beginning of the next revolution. Alternatively, assuming that the changes in the elements during the complete manoeuvre are small compared to their nominal values, one can make the approximation $\delta\boldsymbol{\alpha} = k\Delta\boldsymbol{\alpha}$, where $\Delta\boldsymbol{\alpha}$ is evaluated for the nominal orbit. Although less precise, this expression has the advantage of being linear in a_t. On the other hand, for angular intervals covering an incomplete number of revolutions the periodic terms for $\boldsymbol{\alpha}$ would need to be considered. A practical example of this can be seen in the study on low-thrust near-Earth object deflection by Colombo et al. [10].

The determination of δM is both more complicated and more critical for the accuracy of the results compared to the other elements, as detailed in [10]. First of all, δM determines the change of phasing at the CA due to the CAM, which is the main responsible for the modification of the miss distance. Secondly, the phasing of the modified CA after the CAM includes both the change in M coming from Gauss' equations and the modification in mean motion [10]:

$$\delta M = \left(n_f - n_i\right)t_{\mathrm{CA}} + n_i t_i - n_f t_f + \Delta M$$

where n_i is equal to the nominal mean motion, and $n_f = \sqrt{\mu/(a+\Delta a)^3}$. Finally, the previous averaged equations do not provide an analytical way to properly estimate ΔM. Certainly, expressing $\mathrm{d}M/\mathrm{d}t$ in terms of the eccentric anomaly and averaging over one revolution in E will always lead to $\Delta M = 0$, as both angular parameters share the same period. However, ΔM will show significant variations for incomplete revolutions due to the contribution of the periodic terms. Therefore, the non-averaged evolution of the mean anomaly during the incomplete revolution at the end of the thrusting phase has to be studied to properly characterise the phasing at CA. Colombo et al. [10] propose to accurately determine the number of complete revolutions and the angle covered in the last, incomplete revolution during the thrusting phase through the numerical integration of the differential equation relating the angular variable used for averaging (in their case, the true longitude) and time. For the formulation proposed in the current work, this amounts to integrating Eq. (6) between the initial and final time of the low-thrust CAM. The ΔM at the final time can then be obtained from the numerical integration of the last of Eq. (5) during the last, incomplete revolution, which requires expressions for the periodic evolutions of a and e. However, this work does not currently include the derivation of the periodic components for a and e, so the differential equations for a and e are integrated together with the one for M instead. The need to numerically integrate the time law, Eq. (6), and the Gauss' planetary equation for M during the last revolution is what prevents the model from being entirely analytical; however, it still provides the advantage of having to integrate just one differential equation, the eccentric anomaly time law, during the whole manoeuvre and another one, the periodic change in M, just during a fraction of a revolution.

The previous semi-analytical model corresponds to a constant acceleration applied along the tangential direction. A similar behaviour can be obtained with a drag sail, the main difference being that the acceleration would depend on the area-to-mass ratio, the atmospheric density, and the instantaneous velocity. For circular or quasi-circular orbits, both atmospheric density and velocity can be assumed to be constant in magnitude along one revolution, and the previous expressions can be applied directly. For more general cases, the dynamics is evaluated using PlanODyn [11], a semi-analytical propagator based on the single-averaged form of Lagrange and Gauss' planetary equations. PlanODyn also allows to compute the corresponding STM through the integration of the variational equations. This approach can also be applied to solar sails, for which the direction of the acceleration is no longer tangential but depends on the satellite-Sun position vector.

3.1 Control strategy

Because the direction of $\boldsymbol{a}(t)$ is fixed in all the cases considered, the control capacity is limited. The control

parameters for the low-thrust propulsion system would be the magnitude and starting and ending time of the low-thrust CAM, or alternatively, the duration of the thrusting Δt_{CAM} and the lead time Δt_f between the end of the thrusting arc and t_{CA}. For drag or solar sails control is achieved by acting on the area-to-mass ratio, assuming that the spacecraft has sufficient attitude control.

4. Test cases and numerical simulations

In this section, several results for different low-thrust CAM strategies are presented. In all cases, a nominal close approach with the values reported in Table 1 is considered. These values are taken from a previous work by the authors on analytical methods for the design of impulsive CAMs [1], and are based on the orbital elements of PROBA-2 for the spacecraft and statistical data from ESA's MASTER-2009 [12] for the fictitious debris.

Table 1. Keplerian orbital elements at CA for spacecraft and debris

	Spacecraft	**Debris**
$\boldsymbol{a}$ **[km]**	7093.637	7782.193
$\boldsymbol{e}$ **[−]**	0.0014624	0.0871621
$\boldsymbol{i}$ **[deg]**	98.2443	88.6896
$\boldsymbol{\Omega}$ **[deg]**	303.5949	142.7269
$\boldsymbol{\omega}$ **[deg]**	109.4990	248.1679
$\boldsymbol{f_0}$ **[deg]**	179.4986	1.2233

The achievable deflection in the b-plane δb as a function of Δt_{CAM} and Δt_f is represented in Fig. 1 to Fig. *3* for different values of a_t. Thrust acceleration levels vary from 10^{-4} m/s^2 to 10^{-6} m/s^2; as a reference, a thrust acceleration of 10^{-4} m/s^2 corresponds to a force of 100 mN for a 1 ton spacecraft. These results show the practical feasibility of low-thrust CAMs, provided that the manoeuvre begins with a sufficient advance with respect to the predicted t_{CA}. As expected, performing the manoeuvre with a higher lead time reduces the required thrusting time for a given displacement, leading to lower propellant consumption. It is also interesting to note how the effect of Δt_f increases with Δt_{CAM}. Another feature of these solutions is that δb appears to vary nearly linearly with a_t. This was expected from the qualitative analysis of the semi-analytical model, because the change in the orbital elements is linear with a_t, and the displacement with respect to the nominal position is linear in $\delta\boldsymbol{\alpha}$. This behaviour is better appreciated in Fig. 4 and Fig. 5, where the ratio between the displacement and the perturbing acceleration is shown for a Δt_f of 1 and 5 nominal periods of the spacecraft, respectively. All the curves fall together except for values of the acceleration of 10^{-2} m/s^2, which is substantially higher than the current technological limits. The non-linearity of the deflection is also affected by the duration of the

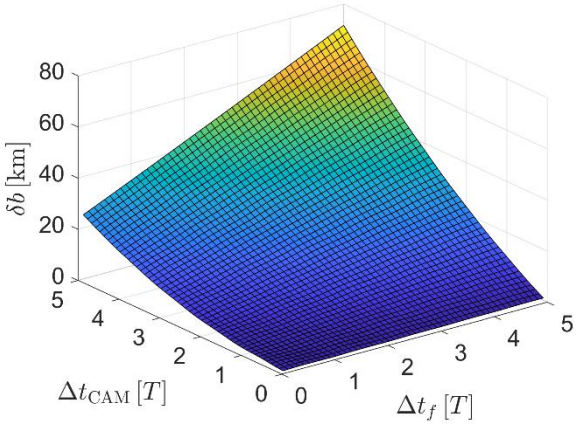

Fig. 1. Deflection in the b-plane for $a_t = 10^{-4}\ m/s^2$ and different values of CAM duration and lead time

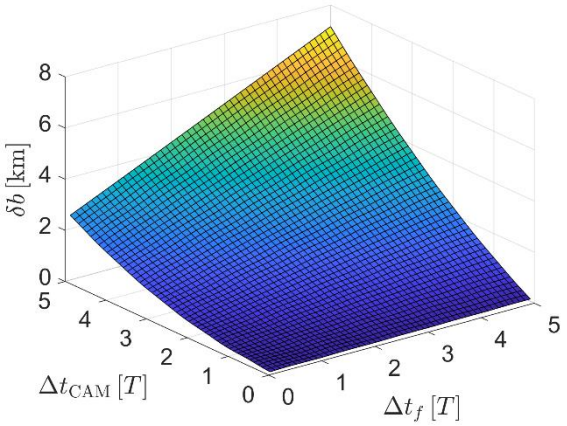

Fig. 2. Deflection in the b-plane for $a_t = 10^{-5}\ m/s^2$ and different values of CAM duration and lead time

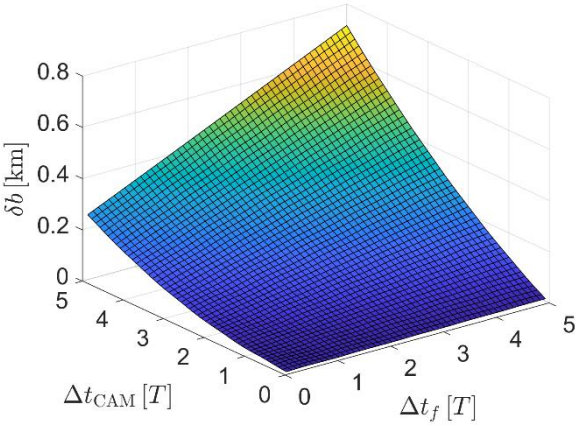

Fig. 3. Deflection in the b-plane for $a_t = 10^{-6}\ m/s^2$ and different values of CAM duration and lead time

manoeuvre, as shown in Fig. 5 for a Δt_f of five periods and a low-thrust acceleration of $10^{-3}\,\mathrm{m/s^2}$. These results sustain the hypothesis of linear dependence of the displacement with the applied acceleration for typical thrust levels and manoeuvre durations.

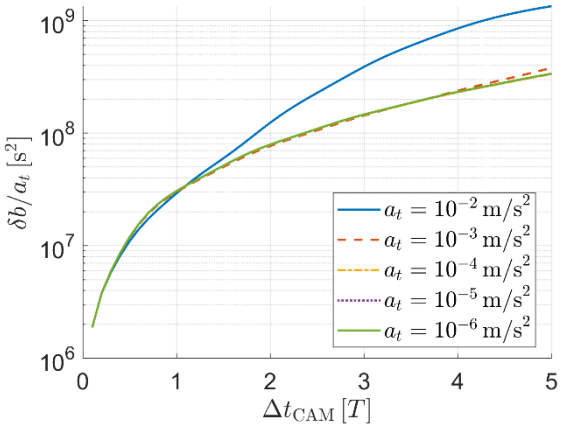

Fig. 4. Evolution of the ratio of displacement and thrust acceleration, for $\Delta t_f = 1$ period and different durations of the manoeuvre

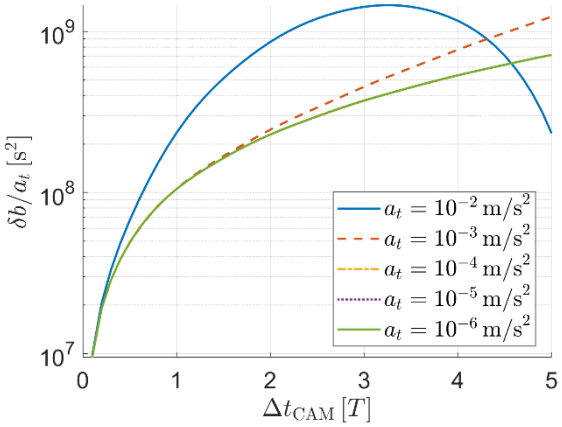

Fig. 5. Evolution of the ratio of displacement and thrust acceleration, for $\Delta t_f = 5$ periods and different durations of the manoeuvre

The choice of a tangential acceleration control law should ensure that most of the displacement is due to changes in phasing, at least for small modifications of the nominal orbital elements. This can be clearly appreciated in Fig. 6, where the evolution of the position of the displaced spacecraft at t_{CA} is represented for CAMs lasting between 0 and 5 periods, for several values of Δt_f and a fixed perturbing acceleration of $10^{-4}\,\mathrm{m/s^2}$. Note that all curves start at the origin and begin separating from it as the corresponding Δt_{CAM} increases. The net changes along the geometry axis ξ are very small, with the displacement advancing dominantly along ζ.

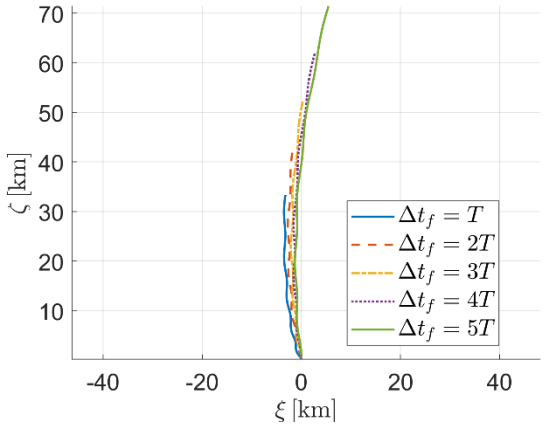

Fig. 6. B-plane representation of the evolution of the displacement with $\Delta t_{CAM} \in [0, 5T]$, for $a_t = 10^{-4}\ m/s^2$ and several Δt_f

The accuracy of the semi-analytical approximation for semimajor axis and eccentricity is now asserted through a relative error defined as:

$$\mathrm{err}(a) = \frac{a_{\mathrm{num}} - a_{\mathrm{sa}}}{a_{\mathrm{nom}}}$$

$$\mathrm{err}(e) = \frac{e_{\mathrm{num}} - e_{\mathrm{sa}}}{e_{\mathrm{nom}}}$$

This error metric has been evaluated for several acceleration levels and durations of the thrust arc (note that both elements remain constant during the coasting arc), and represented in Fig. 7 and Fig. 8 for a and e, respectively. The results confirm that the semi-analytical approach provides a very accurate approximation of the evolution of both elements, for the CAM accelerations and durations under consideration.

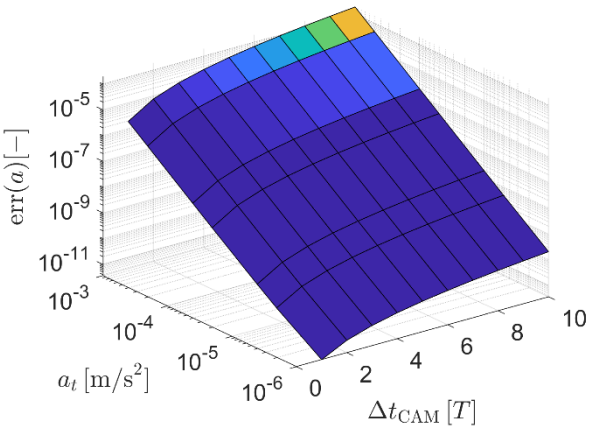

Fig. 7. Relative error of the semi-analytical solution for a

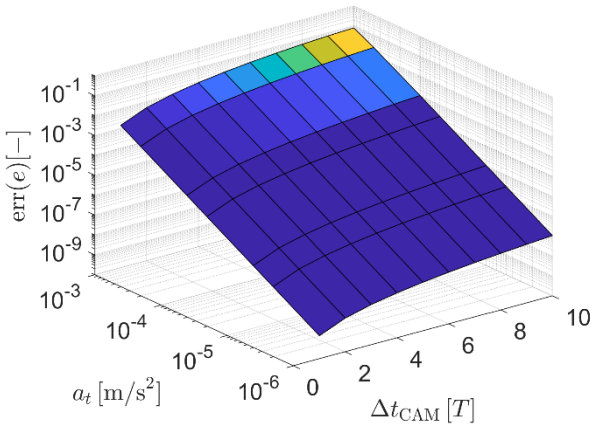

Fig. 8. Relative error of the semi-analytical solution for e

Note that the error for M has not been included in the previous figures. As indicated in Section 3, the averaged Gauss equations do not provide accurate enough information for M, even when including the periodic terms. For this reason, the change in M due to the CAM is computed numerically through the integration of the corresponding Gauss' planetary equation. Searching for a more refined analytical solution for M is left for future works.

As noted in Section 3, although the results presented so far assume a low-thrust propulsion system, they could also be extended to drag sails in quasi-circular orbits, provided that the changes in velocity and atmospheric density along the orbit are small enough. However, the doubt remains about how much do drag and SRP affect the uncertainties of a spacecraft with a significant area-to-mass ratio (e.g. a spacecraft equipped with a sail). Using PlanODyn, the evolution with time of the covariance matrix can be efficiently evaluated, leveraging its single-averaged, semi-analytical underlying formulation. In the following, the evolution of the combined covariance in the b-plane for the same nominal encounter in Table 1 is simulated under the following conditions. It is assumed that orbit determination for both objects is performed at a given time Δt_{OD} before t_{CA}, and that both covariances are statistically independent so that they can be combined through addition. A synthetic covariance matrix at t_{OD} is constructed for each object following the procedure proposed in [1], where the covariance matrix for an arbitrary true anomaly is estimated from the covariance at another point of the orbit. The main idea is to update the orientation of the covariance ellipsoid by numerically propagating the initial covariance and retrieving the new principal directions, while keeping the volume of the ellipsoid by assigning to these eigenvectors the eigenvalues at the original point (where the orbit determination was performed). The reference covariance matrix has been estimated by performing the least-square fitting of SPG4-generated state vectors with the results from a high-accuracy propagator [13]. The particular values used for the numerical tests in this paper, calculated from the TLEs of the catalogue object with NORAD ID 33874, are (units in km and s):

$$\mathrm{C}|_{\mathrm{ref}} = \begin{bmatrix} +1.155460\,10^{-02} & -2.314433\,10^{-03} & -1.173196\,10^{-03} & +4.525295\,10^{-07} & -5.679590\,10^{-07} & -1.094546\,10^{-05} \\ -2.314433\,10^{-03} & +1.914694\,10^{-02} & +1.416720\,10^{-02} & -1.228650\,10^{-05} & -2.553553\,10^{-06} & -3.304939\,10^{-06} \\ -1.173196\,10^{-03} & +1.416720\,10^{-02} & +3.087028\,10^{-01} & -2.875013\,10^{-04} & -8.618777\,10^{-05} & -1.249317\,10^{-06} \\ +4.525295\,10^{-07} & -1.228650\,10^{-05} & -2.875013\,10^{-04} & +2.885067\,10^{-07} & +7.994043\,10^{-08} & +1.151141\,10^{-09} \\ -5.679590\,10^{-07} & -2.553553\,10^{-06} & -8.618777\,10^{-05} & +7.994043\,10^{-08} & +4.599658\,10^{-08} & +1.457009\,10^{-09} \\ -1.094546\,10^{-05} & -3.304939\,10^{-06} & -1.249317\,10^{-06} & +1.151141\,10^{-09} & +1.457009\,10^{-09} & +1.202200\,10^{-08} \end{bmatrix},$$

and the state vector at orbit determination:

$$\mathrm{r_{OD}} = [+6.9687855258\,10^{+03} \quad +2.0930747167\,10^{+03} \quad -8.0909303360\,10^{+00}] \text{ km}$$
$$\mathrm{v_{OD}} = [-1.5353503665\,10^{-01} \quad +4.4753975193\,10^{-01} \quad +7.3566221447\,10^{+00}] \text{ km/s}.$$

Fig. 9 shows the evolution of size and orientation of the covariance ellipse in the b-plane for a range of Δt_{OD}, different levels of uncertainty in the reflectivity coefficient c_R and drag coefficient c_D, and several area-to-mass ratios. In all cases, the debris has $c_D = 2.1$ and $c_R = 1.8$, while the spacecraft is not affected by drag or SRP. The main conclusion regarding uncertainty growth is that the effect of drag and SRP is small except for cases with a combination of very large area-to-mass ratio and uncertainties related to c_R and c_D. Consequently, as a first approximation it would be possible to neglect these two effects when dealing with the propagation of the covariance matrix, and resort instead to the analytical STM in [1]. It is also observed that the covariance tends to align with the time axis of the b-plane as the lead time for the orbit determination grows. This was the expected behaviour, due to the accumulation of phasing-related uncertainties. Because the time axis is also the preferential direction for maximum miss distance CAMs, this will limit the collision risk reductions that can be achieve just by increasing miss distance.

To conclude this section on numerical test cases, some brief comments are made on the possibility of performing CAMs with sails. Although no numerical values will be included here, the authors already studied this problem in detail in [1]. By assuming a simple on/off control law, that is, sail perpendicular or parallel to the

velocity, it was shown that a sail in LEO can perform a CAM just by changing its effective area-to-mass ratio in order to modify the phasing of the CA. There are, however, three key challenges to this approach. The first one is that the spacecraft must be able to modify the effective area-to-mass ratio of the sail, for instance, by changing its attitude. The second one is that there may actually be a worsening of the collision risk during the beginning of the manoeuvre, depending of the geometry of the nominal encounter in the b-plane. And the last one is that the decision to make the manoeuvre should be made several hours or even days before the predicted close approach, reducing the capability of operators to wait for more updated conjunction data messages before making a decision regarding the need to perform the CAM.

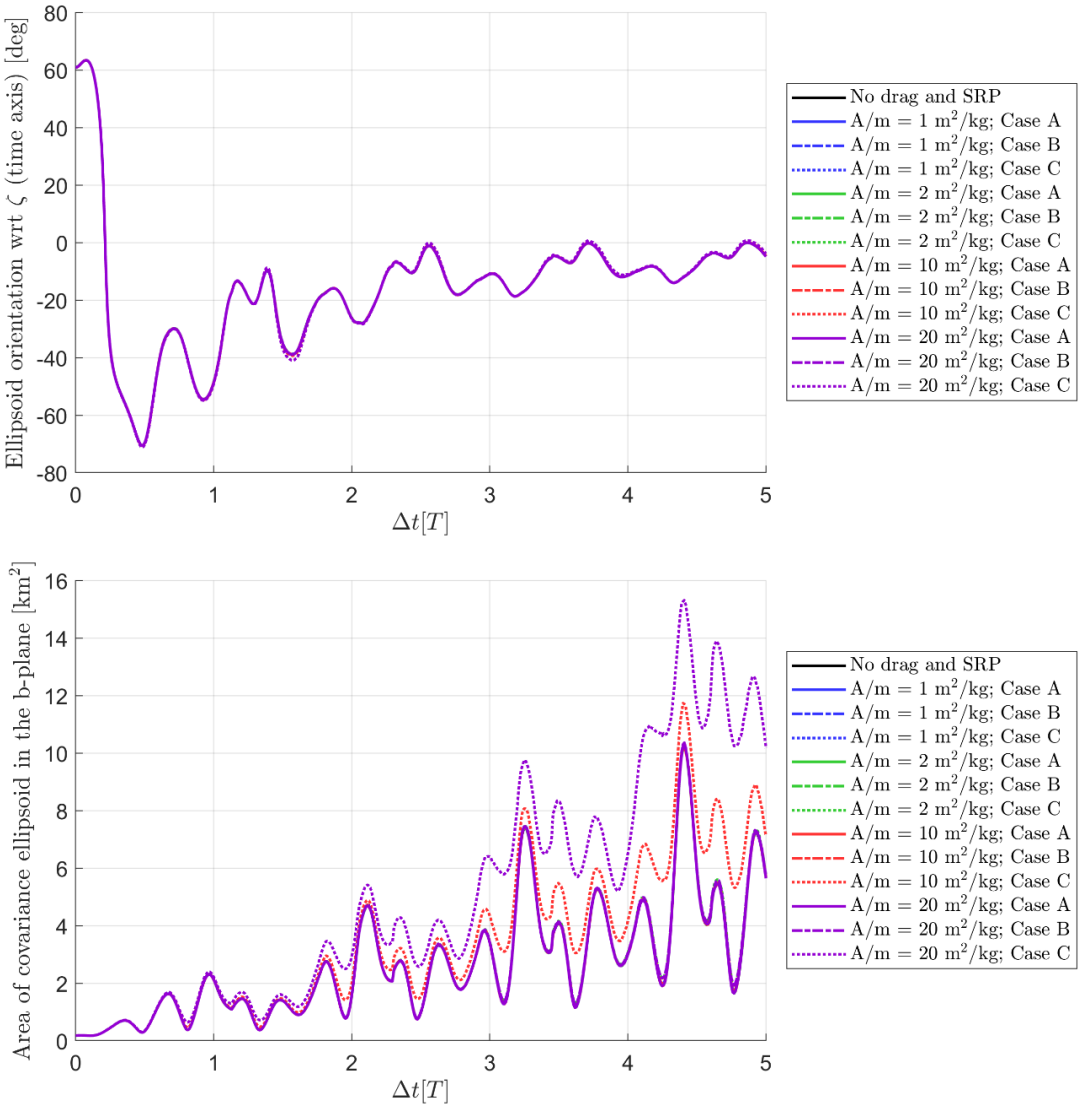

Fig. 9. Orientation with respect to the time axis (top) and area (bottom) of the combined covariance ellipse in the b-plane, for different area-to-mass ratios. Three uncertainty levels are considered for $\sigma_{A/m}$, σ_{c_D}, and σ_{c_R}: A) all zero (no uncertainties); B) 1% of their nominal values; C) 10% of their nominal values

5. Conclusions

A new approach for the design of low-thrust CAMs has been presented, based on analytical and semi-analytical methods and the linearized relative motion equations. Considering previous results for impulsive CAMs, a tangential thrust strategy has been followed. The Gauss' planetary equations have been averaged for a constant tangential thrust over one period of the eccentric anomaly, providing accurate expressions for the mean

evolutions of semimajor axis and eccentricity, and showing that the mean evolutions of inclination, argument of the ascending node and argument of perigee are zero. As already shown in previous works, the averaged equation for M failed to provide enough accuracy to properly describe the phasing change at the CA, requiring two numerical integrations: one during the whole time span to determine the final anomaly, and another during the last (incomplete) period of the CAM to find the final M. The use of this semi-analytical model has allowed to reduce the computational cost while retaining a sufficient accuracy, as it avoids the need to integrate numerically the evolution of all Keplerian elements during the whole duration of the CAM. This feature is particularly important when performing sensitivity analyses or dealing with a congested space with many potential conjunctions.

For those cases where a closed-form approximation was not available, like when using drag or solar sails, the single-averaged, semi-analytical propagator PlanODyn was used to propagate the evolution of the objects and to numerically determine the STMs if needed.

Analysing the evolution of the CAM in the b-plane has confirmed the key role played by phasing, with displacements along the time axis dominating over displacements in the geometry axis. This highlights the importance of planning low-thrust CAMs with sufficient lead time, contrary to impulsive CAMs that can be typically performed in an efficient way up to half an orbital period before the predicted encounter. The numerical simulations have also shown the negligible influence of atmospheric drag and SRP on uncertainty evolution for typical sails sizes, and that the covariance ellipse in the b-plane tends to align with the time axis as lead time grows.

Future developments will include a deeper exploration of the description of δM, trying to find an approximate, time-explicit solution in order to avoid the numerical part of the semi-analytical method. Also, PlanODyn capabilities for the native computation of STMs will be extended.

Acknowledgements

This project has received funding from the European Research Council (ERC) under the European Union's Horizon 2020 research and innovation programme (grant agreement No 679086 – COMPASS).

The authors also want to thank Simeng Huang for her valuable contributions regarding the semi-analytical formulas for the evolution of the orbital elements under a continuous tangential acceleration.

References

[1] J. L. Gonzalo, C. Colombo, and P. Di Lizia, Analysis and design of collision avoidance manoeuvres for passive de-orbiting missions, AAS 18-357, 2018 AAS/AIAA Astrodynamics Specialist Conference, Snowbird, UT, 2018, 18-23 August.

[2] Website of the COMPASS project, https://www.compass.polimi.it/, (accessed 14.10.19).

[3] E. J. Opik, Interplanetary encounters: close-range gravitational interactions, Developments in Solar System and Space Science, vol 2, Elsevier Scientific Publishing Co, Amsterdam, 1976.

[4] M. Vasile, and C. Colombo, Optimal impact strategies for asteroid deflection, Journal of Guidance, Control, and Dynamics, 31, 4 (2008) 858–872. doi: 10.2514/1.33432

[5] J. L. Junkins, and H. Schaub, Analytical mechanics of space systems. American Institute of Aeronautics and Astronautics, Reston, VA, 2009.

[6] R. H. Battin, An introduction to the mathematics and methods of Astrodynamics, AIAA Education series, AIAA, Reston, VA, 1999.

[7] T. N. Edelbaum, Propulsion Requirements for Controllable Satellites, ARS Semi-Annual Meeting, Los Angeles, CA, 1960, pp. 1079–1089.

[8] S. Huang, C. Colombo, and F. Bernelli-Zazzera, Orbit raising and de-orbit for coplanar satellite constellations with low-thrust propulsion, IAA-AAS-DyCoSS4-1-15, 4th IAA Conference on Dynamics and Control of Space Systems, Changsha, China, 2018, 21-23 May.

[9] S. Huang, C. Colombo, E. M. Alessi, and Z. Hou, Large constellation de-orbiting with low-thrust propulsion, AAS 19-480, 29th AAS/AIAA Space Flight Mechanics Meeting, Ka'anapali, HI, 2019, 13-17 January.

[10] C. Colombo, M. Vasile, and G. Radice, Semi-analytical solution for the optimal low-thrust deflection of near-Earth objects, Journal of Guidance, Control and Dynamics, 32, 3 (2009) 796-809.

[11] C. Colombo, Planetary Orbital Dynamics (PlanODyn) suite for long term propagation in perturbed environment, 6th ICATT, Darmstadt, Germany, 2016, 14-17 March.

[12] S. Flegel, J. Gelhaus, C. Wiedemann, P. Vorsmann, M. Oswald, S. Stabroth, H. Klinkrad, and H. Krag, The MASTER-2009 space debris environment model, Fifth European Conference on Space Debris, Darmstadt, Germany, 2009, 30 March – 2 April.

[13] A. Morselli, R. Armellin, P. Di Lizia, and F. Bernelli Zazzera, A high order method for orbital conjunctions analysis: sensitivity to initial uncertainties, Advances in Space Research, 53, 3 (2014) 490-508.